Philosophical Magazine,
Vol. 86, No. 27, 21 September 2006, 4285–4303

Taylor & Francis
Taylor & Francis Group

Internal friction due to negative stiffness in the indium–thallium martensitic phase transformation

T. JAGLINSKI†, P. FRASCONE‡, B. MOORE§, D. S. STONE§ and R. S. LAKES*¶

‡¶Department of Engineering Physics
§Department of Materials Science and Engineering
¶Biomedical Engineering Department
†§¶Materials Science Program
¶Rheology Research Center, University of Wisconsin-Madison, 1541 Engineering Research Building, 1500 Engineering Drive, Madison, WI 53706-1687 USA

(*Received 29 July 2005; in final form 18 November 2005*)

Internal friction and dynamic shear modulus in an indium–21 at.% thallium alloy were measured as functions of frequency and cooling rate using broadband viscoelastic spectroscopy during the martensitic transformation which occurs in this material occurs around 50°C. Microstructural evolution of martensitic bands was captured using time-lapse optical microscopy. The amplitude of damping peaks due to the temperature-induced transformation in the polycrystalline alloy was found to exceed those reported by others for single crystals of similar alloy compositions, in contrast to the usual reduction in damping in polycrystals. The high temperature portion of the damping peak occurs before martensitic bands are observed; therefore this portion cannot be due to interfacial motion. Constrained negative stiffness of the grains can account for this damping, as well as for amplification of internal friction peaks in these polycrystals and for sigmoid-shaped anomalies in the shear modulus at high cooling rates. Surface features associated with a previously unreported pre-martensitic phenomenon are seen at temperatures above martensite-start.

1. Introduction

The dynamics and internal friction of solid-state phase transformations is of great scientific and technological importance. One of the most fascinating phase transformations in structural materials is the martensitic transformation, responsible for the stress–strain hysteresis and the shape memory effect in some metal alloys, notably nickel–titanium (Ni–Ti or Nitinol), copper–aluminum–nickel (Cu–Al–Ni) and copper–aluminium–zinc (Cu–Al–Zn). Additionally, many minerals display a similar type of transformation, referred to as a ferroelastic transformation [1], which is associated with a stress–strain hysteresis and in some cases the shape memory effect as well. This transformation is important technologically as shape memory alloys, especially Ni–Ti, are making their way into commercial application, finding

*Corresponding author. Email: lakes@engr.wisc.edu

Philosophical Magazine
ISSN 1478–6435 print/ISSN 1478–6443 online © 2006 Taylor & Francis
http://www.tandf.co.uk/journals
DOI: 10.1080/14786430500479738

uses in the biomedical industry as stents and orthodontics. Scientifically, a broader understanding of the mechanical properties of these types of transformations aids our general understanding of material physics and will enable expanded practical application.

The present study is concerned with the causal mechanisms of the observed internal friction peak which occurs in the vicinity of martensitic phase transformations. Here, we use the indium (In)–thallium (Tl) binary alloy system as the model system, where alloys of up to 31 at.% Tl are known to undergo a reversible martensitic phase transformation from a high temperature fcc structure to a low temperature fct structure. Specifically, In–21 at.% Tl specimens, which nominally undergo the martensitic transformation around 50°C, will be studied. These alloys have received attention due to observed shape memory effects as well as high mechanical damping. Work has been done on single crystals [2–7], polycrystals of varying composition [8, 9] and on thin films [10]. The crystallography of this system has been explored in detail [11] and the transformation in single crystals has been studied via video photography and X-ray methods [12, 13]. In general, previous work in this alloy system has been driven by the desire to determine the martensitic reaction pathways and kinetics. From a technological standpoint, these In–Tl alloys have not received much application due to their low melting point, yield stress and stiffness. Theoretical descriptions of the structural changes in this system have been used to help study other shape memory materials possessing similar solid-state phase changes [14].

Some analyses exist for the internal friction peak associated with martensitic phase transformations and are intended to explain general phenomena observed in the internal friction signature attributed to the martensitic transformation, such as (i) increasing peak magnitude with increasing cooling rate, (ii) increasing peak magnitude with decreasing test frequency, and (iii) the hysteresis between the location of the internal friction peak during transient heating and cooling [15, 16]. Many proposed causal mechanisms have been reviewed by Zhang *et al.* [16], Van Humbeeck *et al.* [17] and Fung *et al.* [18]. Most theories are based on the creation and motion of twin boundaries during the transformation. For example, Zhang *et al.* [16] obtained the following relation for the magnitude of the internal friction peak:

$$\tan\delta = A(\dot{T}/\omega)^n. \tag{1}$$

Here, $\tan\delta$ is the maximum value of the internal friction peak, A and n are material dependent constants, $\dot{T}$ is temperature with the dot indicating a time derivative, and ω is the angular frequency in rad s^{-1}. Such theories do not explain observed increases in internal friction prior to martensite formation, peak asymmetry, or the fact that polycrystals exhibit larger, sharper peaks than single crystals.

Contrary to the traditional use of interfacial motion to explain the observed internal friction behaviour, it is hypothesized that grains within a polycrystal undergoing a martensitic (or ferroelastic) phase transition can possess negative moduli below a critical temperature. Internal friction peaks arise then due to competition between positive and negative stiffness portions of the polycrystal. The notion of negative moduli is an outgrowth of the prior use of negative stiffness in composites. Negative stiffness is defined as a reversal in the usual directional relationship between deformations and causal forces and has been utilized in

composite materials where low volumetric concentrations of negative stiffness inclusions were constrained by a positive stiffness matrix [19–21]. In these composites, negative stiffness in the inclusions was achieved through the ferroelastic phase transformation in vanadium dioxide (VO_2) which occurs at a temperature of 68°C. The cast composites displayed internal friction peaks and shear modulus anomalies, in which the mechanical damping was greater than that of either constituent. It was demonstrated [22] with isotropic composite theory that proper balance between the positive and negative stiffness phases can result in arbitrarily large values for the internal friction and stiffness of the bulk composite material. Negative structural stiffness and large enhancements in mechanical damping have been demonstrated experimentally by Lakes [23] in a composite unit cell containing a buckled tube.

The rationale for the existence of negative stiffness arises from established theory and observed material behaviour. Many materials which display ferroelasticity, or a hysteresis in the stress–strain curve (often called pseudoelasticity), display a decrease to zero of one or more of the moduli, attributed to the softening of the phonon modes associated with these moduli. For the In–Tl model system, the $1/2(C_{11} - C_{12})$ shear modulus tends to zero as the martensitic transformation temperature is approached during heating or cooling [4, 5]. Upon cooling through the critical temperature, the material breaks up into bands, visible as the twin structures associated with martensitic reactions. The formation of bands is traditionally understood in the context of the Landau theory [24], in which, as temperature T is lowered, an energy function $F = \varepsilon^6 - \varepsilon^4 + (T + 1/4)\varepsilon^2$ (figure 1) with a single minimum gradually flattens, then develops two minima (the double well function). Since the curvature of this energy profile represents a modulus, the flattening of the curve corresponds to a softening of the modulus toward zero at a critical temperature T_c. Below T_c, the relative maximum between the two potential wells represents

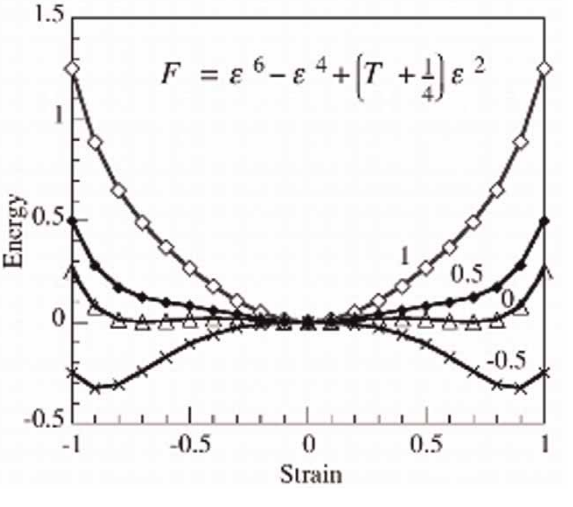

Figure 1. Energy versus strain according to the Landau theory for phase transformation at normalized temperatures 1, 0.5, 0, and −0.5. At high temperature, the energy profile is concave up corresponding to stable equilibrium. When the curve becomes concave down at the origin, equilibrium is unstable, and the material forms bands.

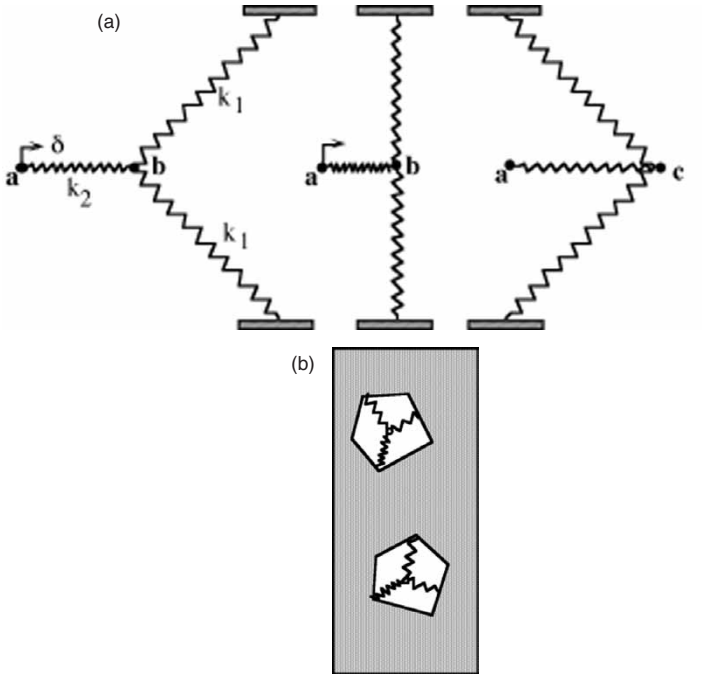

Figure 2. Illustration of negative stiffness. (a) Linear elastic spring model in unstretched condition, (b) preloaded and unstable configuration to (c) snap-through to a new stable position. (d) For phase-transforming inclusions in a matrix, the springs represent interatomic bonds.

negative stiffness. This condition is unstable, so the material forms bands of material with strains of opposite sign corresponding to the new relative minima. However, constraint on the surface displacement of a region of material confers stability, allowing negative stiffness. For example, an isotropic inclusion under rigid constraint is stable provided it is strongly elliptic, which allows a range of $-\infty < E < \infty$ for Young's modulus E and $-4G/3 < B < \infty$ for the bulk modulus B; the shear modulus $G > 0$ [25]. Thus, in a polycrystal, it is hypothesized that negative stiffness in individual grains is stabilized by the surrounding grains.

Negative stiffness behaviour can be visualized with a set of positive stiffness springs arranged in the geometry shown [26] in figure 2. A negative stiffness situation is obtained by applying enough displacement to point **a**, forcing the springs into the unstable equilibrium configuration shown in figure 2b. If k_2 is small, a perturbation of point **b** away from k_2 will cause the system to "snap-through", a phenomenon indicative of negative stiffness. If the restoring force of spring k_2 is large enough to balance the unstable, preloaded k_1 springs the system can have a high structural stiffness. For real materials, the restoring spring, k_2, is replaced by a constraining material which can be the matrix of a designed composite as demonstrated earlier, or the alloy surrounding constrained grains which have negative stiffness below the martensitic transformation temperature. These grains can be modelled as the spring elements. The composite or the alloy, then, contains regions of negative stiffness surrounded by a positive stiffness solid.

The present study explores the mechanical behaviour of In–Tl as a function of temperature, rate of temperature change, and frequency. Specifically, shear modulus and internal friction (expressed as $\tan\delta$) are determined. Concurrently, the formation and disappearance of martensitic bands is evaluated by optical microscopy. The motivation is to test the hypothesis that constrained grains within the polycrystalline metal can attain negative stiffness. If this is indeed the case, negative stiffness in a heterogeneous solid, as discussed above, can give rise to enhancement of the internal friction in a regime where there is balance between positive and negative stiffness. In–Tl was chosen in this study because the bands or domains are rather large. Therefore there are relatively few bands in a grain, facilitating constraint of band formation by neighbouring grains. By contrast, Ni–Ti has a band size of about 20 nm, so constraint on band formation will be minimal.

2. Experimental methods

2.1. *Sample preparation*

Indium wire (Alfa Aesar, 99.9985% metals basis) and thallium granules (Alfa Aesar, 99.999% metals basis) were measured using an electronic balance into the appropriate amounts to create an In–21 at.% Tl alloy. The elements were conventionally cast by melting in a Pyrex beaker inside a muffle furnace at 400°C, swirled to create even mixing, and then poured into a steel mould. The mould cavity was rectangular (with tapered surfaces to allow easy removal) and measured 8.0 cm long, 1.9 cm wide and 1.5 cm deep. Samples were cut using a low speed abrasive saw from the cast ingot into rectangular cross sections, typically on the order of $3 \times 4 \times 30$ mm.

2.2. *Internal friction measurements*

Specimens were tested in torsion using broadband viscoelastic spectroscopy (BVS) as outlined by Lee *et al*. [27] with refinements to the temperature control and added ability to measure slow, large amplitude free end deflections of the cantilevered specimen. Samarium–cobalt magnets were glued to the specimen using cyanoacrylate super glue to generate torque via the action of a Helmholtz coil. The fixed end of the sample was mechanically clamped by tungsten adapters and set screws. Constant frequency tests with variable temperature were conducted at various frequencies well below the specimen resonance (typically about 2 kHz). Maximum surface strain due to the applied torque was less than 10^{-5}. This strain is well below the yield point so any effects of plasticity would be indirectly related to the transformation process. Samples were heated via a resistive microtube furnace wound with Ni–Cr heating wire, and cooled by flowing air through a liquid nitrogen bath. Heating/cooling rates are indicated in the pertinent figures. Sample temperature was measured using a type-K (Omega) thermocouple attached near to, but not in contact with the base of the sample; its voltage was recorded by a digital oscilloscope.

Internal friction ($\tan\delta$, with δ as the phase angle between stress and strain) and shear modulus measurements were taken using a Stanford Research Systems lock-in amplifier (SR850 DSP) by measuring the phase angle between the sinusoidal torque

and displacement signals as well as signal amplitude. Laser spot position was measured by a wide-angle, two-axis photodiode position sensor (Pacific Silicon Sensor Inc. DL100-7PCBA, Westlake, CA) with a detector area of 1 cm^2. The high frequency, small amplitude component of the deflection signal was detected with a split diode light sensor and measured using the lock-in amplifier. Large, low-frequency deflections of the free end of the cantilevered specimen, due to any slow effects such as thermal drift or material instability, were recorded from the detector output voltage using a digital oscilloscope for the horizontal (torsion) and vertical (bending) directions.

2.3. *Microstructural analysis*

Optical studies of the microstructure were undertaken to measure grain size and observe the microstructure as a function of temperature. Since these particular alloys are very soft (one can indent the alloy with a fingernail), care was taken when using polishing techniques to avoid smearing, scratching, and retention of polishing grit; in particular only fine grit SiC abrasive disks (finer than 600) were used. Specimens for polishing were potted in Buehler Sample-Kwik epoxy. To prevent reaction of cold water with the specimen [28] dish soap was used as a lubricant during polishing. For fine polishing, suspensions of 1.0 and 0.3 μm alumina powders in soap on Nylon polishing cloths were utilized. In-between polishing steps, the sample was cleaned using ultrasound in ethanol.

After polishing, the specimens were prepared for observation in an optical microscope by first pressing them against a polished brass block which was heated up to 90°C on a hot plate mounted on the bottom platen of a Carver hydraulic press. Once the block was at temperature, the polished In–Tl specimen was placed on the polished face of heated steel block (polished faces together), and pressed with 0.8 tonnes (over a 3 cm diameter) for approximately 45 minutes. After this, the pressure was released and the specimen removed and allowed to cool to ambient temperature. This procedure results in a smooth surface above 90°C and allows the martensite laths to become visible upon cooling.

After the initial cooling, the specimen was thermally cycled in the microscope with the heating stage shown in figure 3. The inner alumina ring was wound with Ni80–Cr20 heating wire (10 gauge, 6.50 Ω/ft, Omega) and fixed in place between the outer and inner ring using high temperature ceramic stove and gasket cement (Rutland Products). An alumina base plate was used to minimize heat flow to the microscope sample stage. An access hole was drilled into the epoxy puck just below the surface to allow the thermocouple to be in direct contact with the metal, and the thermocouple was coated with thermally conductive grease (Omegatherm 201, Omega). Thermal gradients were minimized by placing a glass cover piece (a 75 mm diameter glass window with antireflective coating (Edmund Optics, Tech Spec) for the cover window) over the entire heater and insulating the remaining space between the heater and glass with mineral wool insulation. Power was provided with a variable AC power supply until the desired temperature was reached. Once heated, the specimen was monitored as it cooled using a Nikon Eclipse 80i light microscope (using reflected bright field) with a Nikon DXM1200F digital camera and Nikon v.2.63 Act-1 software. The software was set to automatically take micrographs every 5 seconds, while temperature was monitored using a type-K thermocouple and

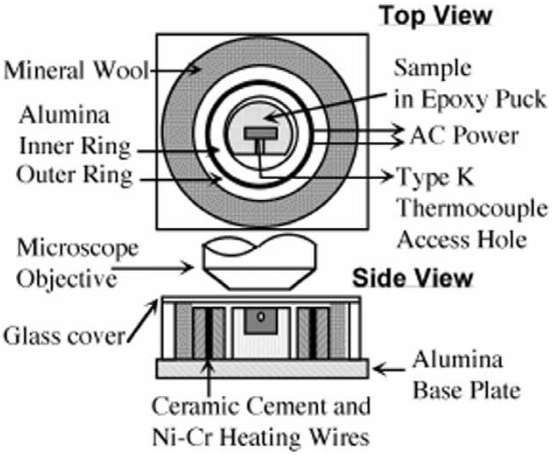

Figure 3. Optical heating stage. The microscope nosepiece was above the glass cover in the side view.

recorded manually as each micrograph was taken. The cooling rate was 2 to $3^{\circ}\mathrm{C\,min^{-1}}$, similar to the rate in the internal friction studies.

3. Results

3.1. *Microstructural analysis*

Figure 4 shows a series of low-magnification micrographs of a polished but unetched cross-section from the same piece of In–21 at.% Tl material characterized for internal friction (see figures 5, 6, 8 and 10). The volume of this specimen was about 8×10^{-3} ml. These micrographs disclose the grain size to be very large, with only a few grains spanning the cross section in any direction. Furthermore, figure 4 illustrates the time–temperature surface relief evolution as the specimen was cooled from a temperature of 80°C. Micrographs were taken at a rate of 5 frames per second with a cooling rate of about $2.7^{\circ}\mathrm{C\,min^{-1}}$ between 60 and 50°C. Full time-lapse movies can be obtained on the web [29]. Since the material was pressed flat at high temperature it has no surface relief above its transformation temperature, as shown in figure 4a. As the sample is cooled surface relief develops revealing the distinctive twinned martensitic pattern. Even up to 80°C, portions of the specimen, mostly at the edges, retained their surface relief.

Optical investigations revealed that the transformation is associated with the expected formation of bands or twins. The prominent feature of the transformation is the formation of long wavelength twins which appear abruptly over a very narrow temperature window. Upon close examination of the time lapsed micrographs, these large twins first appear at 50°C on the far right of the large central grain (figure 4d), with the entire specimen cross section fully transformed by 48°C. Appearance of these structures is extremely sudden, spanning the entire grain.

In addition to the martensite, and in contrast to it, a precursor structure is seen prior to the martensitic transformation. Well above 50°C, this precursor structure

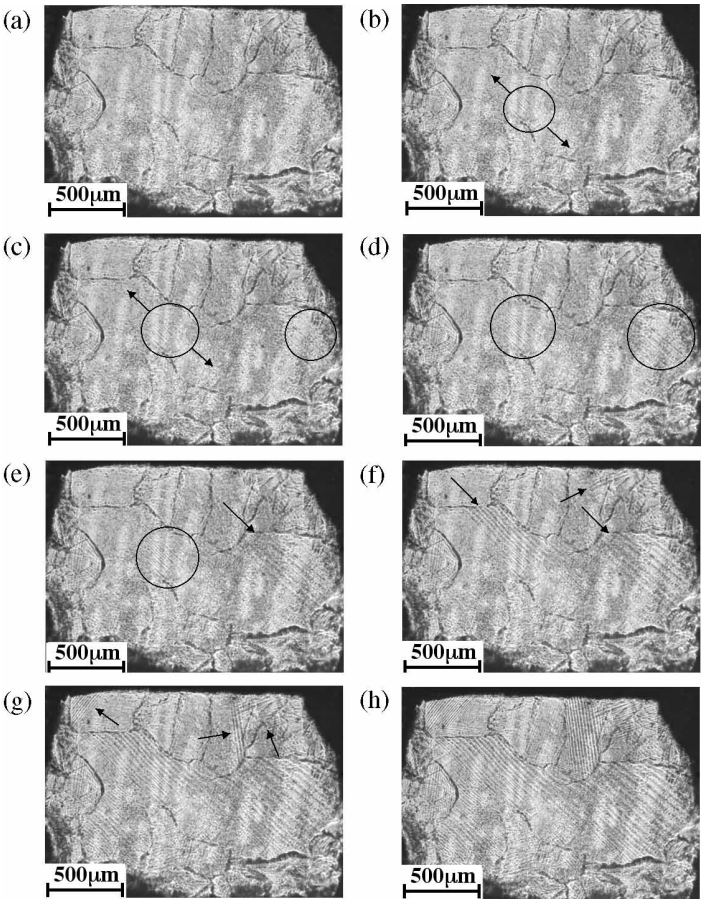

Figure 4. Micrographs of the cross section (approximately 2.5×2 mm) of a nominally In–21 at.% Tl alloy specimen during cooling at (a) 66.0, (b) 60.1, (c) 54.0, (d) 50.1, (e) 49.9, (f) 49.6, (g) 48.0 and (h) 24°C. The circled areas indicate fine precursor bands in some regions before the transformation temperature of 50°C has been reached. Arrows indicate the presence of twin structures after (below) 50°C.

appears as low-contrast surface streaking, or fine scale bands in some grains. For the sample shown in figure 4, these streaks or bands begin to appear around 62°C, but the evolution of these features is very gradual and an exact start temperature cannot be identified at this magnification. Unlike the sudden expansion of the martensite, this structure does not span the entire grain. Some of these bands are indicated by the large circles shown in figures 4b–4d. It is noteworthy that these structures occur in some but not all grains. Furthermore, once the martensite transformation begins the martensite laths tend to supersede any previously existing precursor structure.

Lastly, the transformation exhibited no temperature cycle dependence. Several runs were conducted at similar cooling rates on the specimen shown in figure 4, and in all cases the appearance of the precursor structure and the martensite occurred at the same temperatures. Furthermore, the twin structure was reversible with the same twin structure reappearing for each thermal cycle.

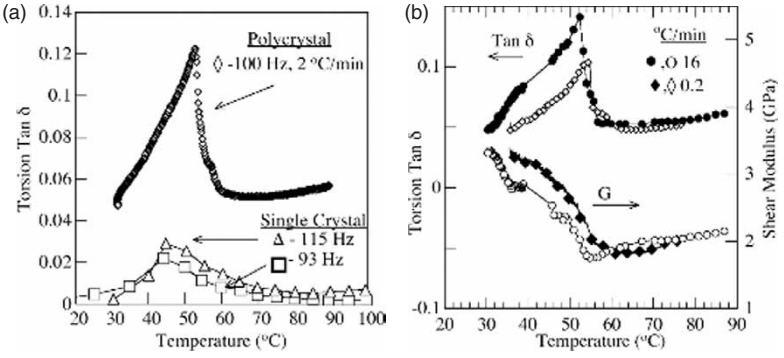

Figure 5. (a) A typical internal friction signature during cooling at 100 Hz for the polycrystalline samples in the present study in comparison to single crystals of similar composition from Li *et al.* [7], and (b) internal friction and shear modulus for the polycrystalline sample at two different cooling rates.

3.2. *Internal friction*

To explore the role of the martensitic transformation on mechanical behaviour the modulus and internal friction were examined. Figure 5a shows the typical internal friction signature for the present In–21 at.% Tl alloy as the specimen was cooled from more than 90°C at a constant frequency of 100 Hz. For comparison, data for $\tan\delta$ from a single crystal from Li *et al.* [7] have also been included in figure 5a. The internal friction signature of the polycrystalline specimen differs markedly from that of the single crystal in several ways: (i) the inclusion of a high temperature background due to the presence of grain boundaries [30, 31], (ii) the sharpness of the onset of the peak and (iii) relative to the background, the polycrystalline peak is greater in amplitude than that for the single crystal. In the present study the first resonant peak of the specimen was about 2 kHz, with all tests (except the broadband results in figure 8) conducted well below resonance. The large peak in the present polycrystal differs from the usual internal friction peaks in polycrystals, as follows. Peaks in polycrystals are broader and weaker, due to a superposition of contributions from different crystals to the overall mechanical behaviour [32]. Moreover, the observed peak is markedly asymmetrical in contrast to nearly symmetrical peaks typically observed. The large damping observed is not surprising in a material of low melting point. Figure 5b displays curves for the specimen shear modulus and $\tan\delta$ over a range of temperature at two different cooling rates (driving frequency of 100 Hz). Dynamic modulus measurements were made concurrently with those for $\tan\delta$. In this series, the shear modulus of the polycrystalline metal displays the same general shape as that reported for single crystals [4, 5].

Figure 6 demonstrates the effect of cooling rate on the amplitude of the internal friction peak through the phase transformation on an expanded scale temperature. Curves for cooling rates of 0.2 and 16°C min^{-1} are the same as those shown in Figure 5b. In general, a higher cooling rate increases the amplitude of the peak and causes a slight downward shift in the maximum temperature of the peak. Observe that the rise in internal friction occurs well before (at higher temperature than) the martensitic transformation at 50°C, witnessed in the present optical investigations. Since there is no martensite above 50°C the internal friction in this regime is not due

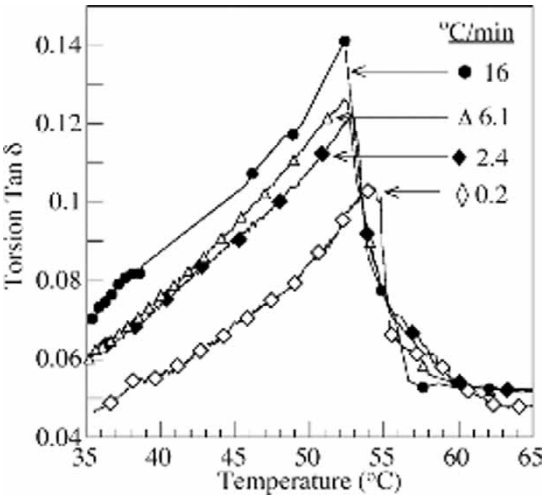

Figure 6. Enlarged view of internal friction peaks to show effect of cooling rate on peak height and peak temperature.

to the motion of interfaces between bands. Interestingly, at about the temperature where the martensite first appears, according to microscope observations, $\tan\delta$ has begun to decrease in our internal friction experiments. (Again, for comparison, the rate of cooling in the time lapse photography experiments was about $2.7^{\circ}\mathrm{C\,min^{-1}}$ at temperatures between 60°C and 50°C and can be compared directly with the curve at $2.4^{\circ}\mathrm{C\,min^{-1}}$ in figure 6, in which the peak occurs at about 53°C.

To examine the experiments for reproducibility and since the first one was sectioned for optical microscopy, a second specimen was made and tested. Presumably, this specimen had a marginally higher concentration of thallium because it had a higher transformation temperature. This system has a steep phase boundary so the transition temperature is highly sensitive to composition. Other than the higher transformation temperature, the internal friction behaviour and the structural transitions were similar to the behaviour of the first specimen. Specifically, the martensite start temperature coincided closely with the maximum of the internal friction but not the onset of the internal friction peak. For this reason we did include the bulk of the data from the second specimen. However, of specific interest, a sigmoid shaped anomaly in the shear modulus was observed at a rapid cooling rate not achieved in the experiments with the first specimen (figure 7). This effect is not predicted by available theories for martensitic transformations. Such a sigmoid shaped anomaly is known theoretically and experimentally in designed composites with inclusions of negative stiffness as previously mentioned.

Figure 8 shows the temperature and frequency dependence of torsional $\tan\delta$ for the polycrystalline specimen with dimensions of $37.5 \times 3.3 \times 2.4\,\mathrm{mm}$ presented in figure 4. Data for figure 8a were obtained by bringing the specimen to a steady state temperature for 30 min and measuring $\tan\delta$ at frequencies of 1, 3, 10, 30, 100 and 300 Hz. Data for figure 8b were taken by scanning frequency over 7 decades, including the first and second structural resonances, on the same specimen at constant temperature. Humps are observed in the broadband curves below the

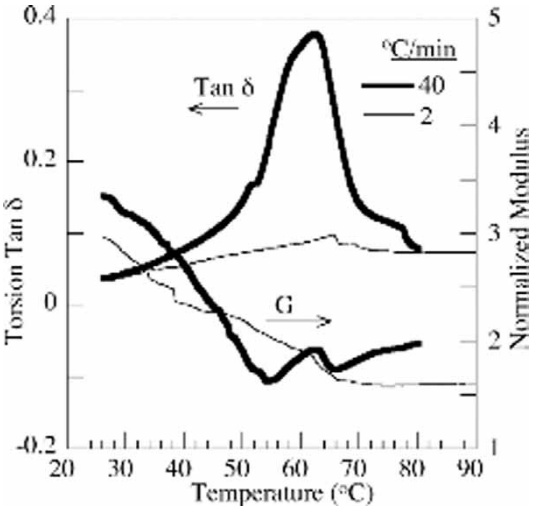

Figure 7. Internal friction peaks and normalized shear modulus, G, showing the development of sigmoid shape anomalies in the shear modulus at high cooling rates.

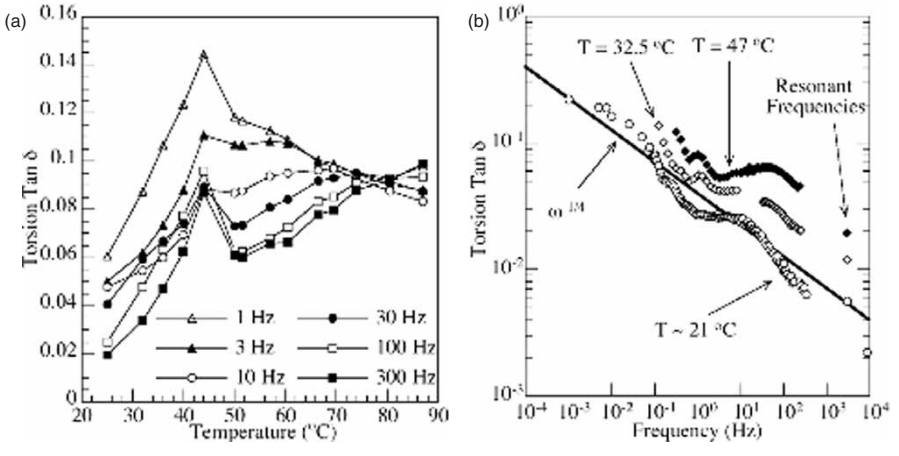

Figure 8. (a) Tan δ as a function of steady-state temperature at various frequencies, and (b) tan δ as a function of frequency at various temperatures for polycrystalline In–21 at.% Tl alloy.

transformation temperature. Also shown in figure 8b is a power law model for tan δ of the form shown as equation (1). The humps in this frequency range are in contrast to the $A\omega^{-n}$ roll-off of tan δ with increasing frequency observed in materials [33], which do not undergo a phase transformation but which, like In–Tl, have a tan δ of large magnitude associated with a low melting point.

A trend of increasing damping peak amplitude with increasing cooling rate and decreasing with driving frequency was observed. As shown in figure 9a, for a constant cooling rate of $2^{\circ}\mathrm{C\,min^{-1}}$ peak amplitude decreased with increasing frequency and peak amplitude increased with increasing cooling rate at constant frequency. However, it is clear from figure 9a that the detailed behaviour does

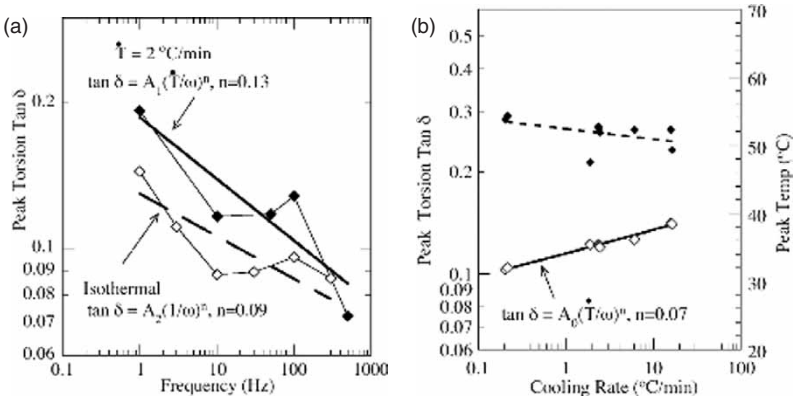

Figure 9. (a) Plots of peak $\tan\delta$ as functions of frequency for a cooling rate of $2^{\circ}\mathrm{C\,min^{-1}}$ (closed diamonds) and isothermal conditions from figure 9a (open diamonds), and (b) a plot of peak $\tan\delta$ and peak temperature for all experiments on the In–21 at.% Tl specimen shown in figures 5–7. The curve fit for $\tan\delta$ is of the form shown in as equation (1); a power law was used to fit the peak temperature.

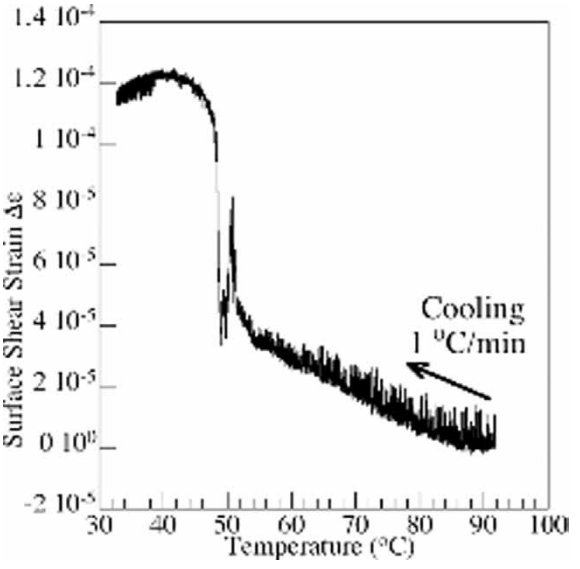

Figure 10. Change in the torsional surface shear strain as the polycrystal was cooled from above 90°C. Structural instability occurs during the phase transformation, near 50°C.

not follow true power law behaviour as is evidenced by the humps in $\tan\delta$ with increasing frequency (which also appear in the broadband results of figure 8b). This is not entirely unexpected as experiments usually only encompass narrow frequency or cooling rate windows. It was also observed that a hysteresis existed during transient heating and cooling, furthermore if the heating or cooling rate was reduced to zero the internal friction appeared to approach a background value.

Figure 10 illustrates the macroscopic structural response of the specimen during the cooling portion of a thermal cycle at about $1^{\circ}\mathrm{C\,min^{-1}}$. In figure 10, the change

in surface shear strain as the specimen cooled reveals a structural instability as the phase transformation occurs. Initially, only slow monotonic drift due to differential thermal expansion is observed. As the specimen is cooled through the transformation temperature the entire specimen undergoes a spontaneous torsional strain. This is called spontaneous strain in the parlance of ferroelastic materials. This manifestation of structural instability occurs at the same martensitic transformation temperature of about 50°C as disclosed by the present optical microscopy. Related instability has been reported for composites intentionally designed to have instability. Tin–vanadium dioxide (VO_2) composites containing 5 vol.% VO_2, which were predicted to be unstable, displayed large aperiodic thrashing during cooling [20] where instability resulted from loss of balance between the negative and positive stiffness phases.

4. Analysis

The role of negative stiffness in heterogeneous materials can be most easily appreciated in the context of the Hashin–Shtrikman formulae for two phase composites. The lower bound formula for the shear modulus G_L of an elastic composite is,

$$G_L = G_2 + \frac{V_1}{(1/(G_1 - G_2)) + ((6(K_2 + 2G_2)V_2)/(5(3K_2 + 4G_2)G_2))}, \tag{2}$$

in which K_1, G_1 and V_1, and K_2, G_2 and V_2 are the bulk modulus, shear modulus and volume fraction of phases 1, and 2, respectively. This represents a bound in the elastic case. Viscoelastic materials are analyzed by allowing moduli to become complex following the correspondence principle [34]. The upper and lower Hashin–Shtrikman bound formulae are attained exactly for bulk modulus with a morphology in which the composite is filled with coated spheres of different size. The shear modulus formula is attained exactly by hierarchical laminates and approximately in the coated sphere morphology. If the inclusions have negative stiffness, the formula is no longer a bound but it is still an exact solution. In principle, as shown in figure 11a, it is possible to tailor the negative stiffness of one phase relative to the positive stiffness of the other to give rise to a large peak in internal friction [22]. Negative shear modulus of an unbounded region of material is unstable; such a region forms a band or domain structure, so the negative stiffness is not usually observed.

In the following, a similar analysis is developed to predict the behaviour of polycrystals containing grains with negative modulus. In a polycrystalline material of cubic symmetry, the bulk modulus K and two shear moduli G_1 and G_2 are given in terms of the tensorial moduli as:

$$K = \frac{1}{3}(C_{11} + 2C_{12}) \tag{3}$$

$$G_1 = \frac{1}{2}(C_{11} - C_{12}), \quad G_2 = C_{44}. \tag{4}$$

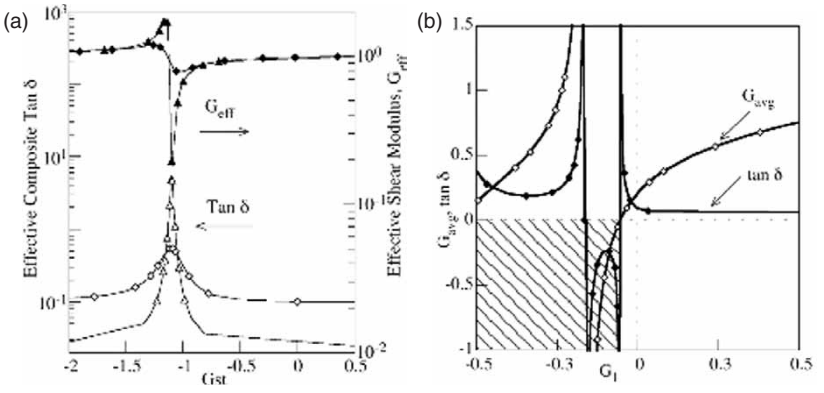

Figure 11. Theoretical plots of aggregate properties when a portion of the material is allowed to have negative stiffness. (a) Theory for isotropic composites comprised of 1% concentration of coated spheres and an inclusion modulus becoming increasingly negative. One composite has a matrix $\tan\delta$ of 0.025 (triangles) and the other a $\tan\delta$ of 0.1 (diamonds) (b) Theory for a polycrystalline aggregate with $\tan\delta_2 = 0.1$, in which the shear modulus G_1 can become negative. The hatched region indicates material instability and subsequent formation of bands.

The properties of the polycrystal depend on the tensorial moduli and on the geometry of the constituent crystals; however, the properties may be bounded [35] by the Voigt formula G_V and the Reuss formula G_R.

$$G_V = \frac{1}{5}(2G_1 + 3G_2), \tag{5}$$

$$G_R = \frac{5G_1G_2}{2G_2 + 3G_1}. \tag{6}$$

More stringent upper, G_U, and lower, G_L, bounds for cubic materials are given by

$$G_L = G_1 + 3\left\{\frac{5}{G_2 - G_1} + 4\frac{3}{5G_1}\frac{K + 2G_1}{3K + 4G_1}\right\}^{-1}, \tag{7}$$

$$G_U = G_2 + 2\left\{\frac{5}{G_2 - G_1} + 6\frac{3}{5G_2}\frac{K + 2G_2}{3K + 4G_2}\right\}^{-1}. \tag{8}$$

Further analyses have also been conducted for materials of lower crystal symmetry [36].

Allowing the shear modulus G_1 to become negative in equations (5)–(8) provides several predictions for the polycrystalline behaviour. In general, both the Voigt formula, equation (5), and the upper Hashin–Shtrikman formula, equation (8), predict a singularity in internal friction and a sigmoid shaped curve for the polycrystalline shear modulus. Conversely, the lower Hashin–Shtrikman formula, equation (7), and Reuss formula, equation (6) provide lower bounds in which the aggregate shear modulus tends to zero as G_1 tends to zero.

To better illustrate the overall behaviour, the average of the upper and lower Hashin–Shtrikman formulae are plotted in figure 11b. As the shear modulus G_1 approaches zero in figure 11b, the aggregate shear modulus drops and the internal

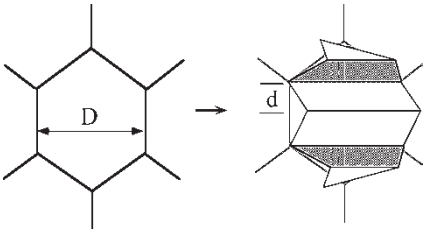

Figure 12. Schematic representation of band formation in an inclusion or a grain as the solid is cooled from above the transition temperature (left) to below (right).

friction increases. This means that the polycrystalline internal friction begins to rise before (at a higher temperature than) the phase change occurs. As G_1 passes through zero and becomes negative, a singularity in the internal friction develops and the polycrystalline shear modulus approaches zero. For G_1 sufficiently negative the aggregate shear modulus becomes negative, indicating instability and the formation of martensitic bands. Once formed, the martensite differs from the high temperature phase; it has a different shear modulus and internal friction, as seen in the experimental results in figure 7. The asymmetric shape of the internal friction peak may be regarded as evidence of this notion.

Negative stiffness usually entails instability, but it is possible for an inclusion in a composite or a grain in a polycrystal to have negative stiffness and be stabilized by the surrounding material. As for shear, in a finite region such as a composite inclusion or a grain in a polycrystal, bands of heterogeneous shear (figure 12) gives rise to an irregular surface, causing deformation to depth on the order of band width d in the surrounding material [37]. This entails a partial constraint on the band formation, hence the possibility that stiffness can become somewhat negative prior to the onset of instability. The resulting energy penalty ΔF is proportional to band width d, the polycrystal shear modulus G, and the grain surface area: $\Delta F = aGD^2d$ [37]. If the bands are relatively large, as they are in In–Tl, the depth of deformation of the surrounding grains, hence the magnitude of the constraint, can be substantial. As for volumetric deformation, the bulk modulus K in the cubic system is given in terms of the compliances S [38] by

$$K = \frac{1}{3(S_{11} + 2S_{12})}. \tag{9}$$

This can be written as

$$K = \frac{1}{3}\frac{1}{((C_{11} - C_{12})^{-1} + 3S_{12})}. \tag{10}$$

However, the modulus $1/2\ (C_{11} - C_{12})$ of In–Tl softens to zero at the transformation temperature [4, 5], and in a constrained system will become negative below that temperature. Therefore the bulk modulus can become negative. This is of interest since a constrained object with negative bulk modulus can be stable as discussed in the introduction.

The present theoretical analysis for composites and polycrystals predicts large peaks in internal friction associated with constituent negative stiffness; however,

there are differences. With regards to material stability, for composites one can titrate the inclusion concentration and stiffness to achieve overall stability. In polycrystals, the predicted internal friction has a singularity, but before it becomes singular, instability occurs.

5. Discussion

In general, the In–Tl alloy exhibited internal friction peaks in the vicinity of the transformation temperature which were qualitatively similar to behaviour reported by others. Specifically, the internal friction tended to increase with decreasing frequency and increasing cooling rate, phenomena which are describable by existing models [16]. However, in the present work several phenomena were observed which cannot be understood in the context of existing theories, but which are consistent with the hypothesis that partially constrained grains within the material exhibit negative stiffness. One may recall that the existence of negative shear moduli is implied by experimental observations of anomalies in torsional internal friction and modulus in Sn–VO_2 composites [19–21]. Negative shear moduli of the inclusions were inferred through comparison of the observed composite behaviour with theoretical predictions; they cannot be measured directly.

Firstly, the high temperature portion of the internal friction peak occurs above the temperature at which martensitic bands are observed. Since there is no martensite in this regime, the internal friction cannot be due to interface motion associated with the martensitic reaction, a main ingredient in such theories. In fact, the appearance of the martensite signals that the maximum $\tan\delta$ has been obtained, after which the internal friction decreases. Interface effects may play a role in the background internal friction at temperatures below the martensitic transformation temperature.

Secondly, the macroscopic structural deformation of the cantilevered sample shows a torsional instability (spontaneous strain) near 50°C (figure 10), the same temperature at which the martensite is observed optically at the surface. This observation corroborates the optical results; it constitutes additional evidence against the idea that motion of interfaces gives rise to the internal friction before the martensitic transformation. Since the spontaneous strain involves the entire specimen, it is unlikely that local permanent deformation of the surface has significantly perturbed the temperature of transformation at the surface.

Thirdly, the polycrystalline solid exhibits a substantially higher internal friction peak than that reported for single crystals with similar compositions and at similar test frequencies. In polycrystals it is known that the broadband high temperature background is elevated, but a large background does not account for the peak magnitude since the maximum $\tan\delta$ is well above the background, and relative to the background is still greater than the single crystal peak. The behaviour of the present indium–thallium is in contrast to the usual situation in which internal friction peaks in polycrystals are broader and weaker, due to a superposition of contributions from different crystals in the material. Since martensitic bands occur in both polycrystals and single crystals, interface theories cannot readily account for the higher peak. Interestingly, the gradual increase in contrast associated with the precursor

bands correlates closely with the gradual increase in $\tan\delta$ that takes place as the temperature is lowered toward the martensite start temperature; it might be, therefore, that the pre-martensitic bands we observe are responsible for the rise in internal friction that takes place as the martensite start temperature is approached, though they only occur in a few grains in the cross section. As a caveat, it is also possible that twin refinement occurs near grain boundaries to maintain compatibility between grains, creating more twin interfaces and subsequently raising the total internal friction in the polycrystal. This explanation would not, however, account for the elevation of internal friction at temperature above the martensite start temperature.

Finally, with regards to negative stiffness, sigmoid shape anomalies in the shear modulus with increasing cooling rate were observed and cannot be accounted for by theories based on interface motion. Negative stiffness is inferred from the present material behaviour through comparison to the Hashin–Shtrikman analysis for polycrystals in which constituent grains are allowed to possess negative stiffness (figure 11). Comparison between the prediction for the polycrystal and the observed sigmoid shape anomalies in figure 7 suggests that portions of the alloy do indeed have negative stiffness. The effect is most pronounced at high cooling rate since there is insufficient time for divergence of the metastable nature of negative stiffness. In particular, Wang and Lakes [39, 40] showed that for a discrete viscoelastic system containing a negative stiffness element that the degree of system metastability affects the overall damping of the system, with an increase in cooling rate decreasing the rate of divergence and providing metastability rather than instability. Thus, for high cooling rates, the negative element can be stabilized for a longer period of time, giving rise to increased $\tan\delta$, and undulations in the shear modulus before the system becomes unstable and reverts to its final stable structure. Although negative structural stiffness has been measured in other systems, direct measurement of a negative shear modulus would be complicated by the need to use a single domain single crystal under hard displacement control.

One notable feature which was observed but is not attributed to negative stiffness behaviour is the broadband internal friction observed in frequency-dependent isothermal experiments. Data in figure 8b resemble the ω^{-n} behaviour observed in materials such as In–Sn [33] and In–Cd [41] which are not in the vicinity of a martensitic phase transformation. It must be noted that the ω^{-n} behaviour referred to here is not the same as the ω^{-n} dependence for peak $\tan\delta$, as in equation (1), referred to earlier. The broadband spectrum therefore has another cause, which is still not well understood.

Lastly, in regards to the precursor structure observed in the present optical experiments, pre-martensitic phenomena are known [42, 43], but most reports deal with diffuse scattering in X-ray or electron diffraction patterns. The authors who report such observations explicitly state that diffuse scattering is not associated with any surface features [44], especially the kind of banding that we observed. Our observations clearly demonstrate surface relief which is not caused by the martensitic reaction but is instead a precursor to it. The structure differs from the tweed microstructure at times seen associated with martensitic transformations [45]. Pre-transformation twinning has been proposed [46] but has not been refuted or substantiated. It must also be noted that surface relief does not always reflect the

true nature of the internal structure [37]. For example, plastic deformation due to processing may give rise to residual stresses in the surface region. Clearly, more work needs to be done to elucidate physical structure and origins of these regions. For example, dependence of properties upon grain size could be studied; however grain size dependence does not influence the present interpretation of results since the optical and mechanical tests were conducted on the same specimen.

6. Conclusions

Existing theories based on interfacial motion (such as twin boundary motion) can account for some general characteristics, such as elevated internal friction in the presence of martensite, of the effect of the phase transformation on the internal friction signature. Several characteristics are not accounted for by such theories but can be understood in the context of negative stiffness of some grains constrained by the surrounding material, analyzed via the theory of polycrystals as heterogeneous media. Specifically, internal friction rises above the transition temperature T_c (revealed consistently by both surface microscopy and bulk spontaneous strain). Therefore the rise in internal friction at temperatures above T_c is not due to martensitic interfacial motion. Also, the polycrystalline solid exhibits an internal friction peak substantially larger than that seen in single crystals. Such amplification of internal friction peaks and the appearance of anomalies in the polycrystalline shear modulus are predicted by the present effective polycrystalline analysis if negative moduli are allowed. The sigmoidal anomalies observed in the shear modulus with increasing cooling rate cannot be accounted for by theories of twin boundary motion but are predicted by theory of polycrystals in which moduli can become negative.

Previously unreported precursor surface relief which precedes the martensitic phase transformation by over 10°C is observed. The exact nature of this phenomenon remains to be elucidated.

References

[1] E.K.H. Salje, *Phase Transformations in Ferroelastic and Co-elastic Crystals* (Cambridge University Press, Cambridge, 1990).
[2] D.B. Novotny and J.F. Smith, Acta Metall. **13** 881 (1965).
[3] B.I. Verkin and I.V. Svechkarev, Soviet Phys. JETP **20** 267 (1965).
[4] N.G. Pace and G.A. Saunders, Proc. R. Soc. A **326** 521 (1972).
[5] D.J. Gunton and G.A. Saunders, Solid St. Commun. **14** 865 (1974).
[6] M. Wuttig, C. Lei, and I. Hwang, J. Physique **46** C10–621 (1985).
[7] J. Li, X. Zhou, and M. Wuttig, Scripta Metall. Mater. **24** 901 (1990).
[8] M.E. de Morton, J. Appl. Phys. **40** 208 (1969).
[9] M. Wuttig and C.H. Lin, Acta. Metall. **31** 1117 (1983).
[10] C.H. Sonu and T.J. O'Keefe, Mater. Characterization **33** 311 (1994).
[11] Z.S. Basinski and J.W. Christian, Acta. Metall. **2** 101 (1954).
[12] Z.S. Basinski and J.W. Christian, Acta. Metall. **2** 148 (1954).
[13] J.S. Bowles, C.S. Barrett, and L. Guttman, Trans. AIME J. Metals **188** 1478 (1950).

[14] K. Bhattacharya, *Microstructure of Martensite* (Oxford University Press, New York, 2003).
[15] W. Benoit, in *Mechanical Spectroscopy Q^{-1} 2001*, edited by R. Schaller, G. Fantozzi, and G. Germaud (Trans Tech Publications, Switzerland, 2001).
[16] J.X. Zhang, P.C.W. Fung, and W.G. Zeng, Phys. Rev. B **52** 268 (1995).
[17] J. Van Humbeeck, J. Stoiber, L. Delaey, *et al*., Z. Metallk. **86** 176 (1995).
[18] P.C. Fung, J.X. Zhang, Y. Lin, *et al*., Phys. Rev. B **54** 7074 (1996).
[19] R.S. Lakes, T. Lee, A. Bersie, *et al*., Nature **410** 565 (2001).
[20] T. Jaglinski and R.S. Lakes, Phil. Mag. Lett. **84** 803 (2004).
[21] T. Jaglinski, D. Stone, and R.S. Lakes, J. Mater. Res. **20** 2523 (2005).
[22] R.S. Lakes, Phys. Rev. Lett. **86** 2897 (2001).
[23] R.S. Lakes, Phil Mag Lett. **81** 95 (2001).
[24] F. Falk, Acta metall. **28** 1773 (1980).
[25] R.S. Lakes and W. J. Drugan, J. Mech. Phys. Solids **50** 979 (2002).
[26] Y.C. Wang and R.S. Lakes, Am. J. Phys. **72** 40 (2004).
[27] T. Lee, R.S. Lakes, and A. Lal, Rev. Scient. Instrum. **71** 2855 (2000).
[28] V. Voort, *Metallography Principles and Practice* (McGraw-Hill, New York, 1984), pp. 136–137.
[29] R.S. Lakes, http://silver.neep.wisc.edu/~lakes/slide.dir/InTl.gif.
[30] D.H. Niblett and J. Wilks, Adv. Phys. **9** 63 (1960).
[31] W.P. Mason, *Physical Acoustics and the Properties of Solids* (Van Nostrand-Reinhold, Princeton, 1958), pp. 272–285.
[32] A.S. Nowick and B.S. Berry, *Anelastic Relaxation in Crystalline Solids* (Academic Press, New York, 1972), pp. 435–462.
[33] R.S. Lakes and J. Quackenbush, Phil. Mag. Lett. **74** 227 (1996).
[34] Z. Hashin, J. appl. Mech., Trans. ASME **32E** 630 (1965).
[35] Z. Hashin and S. Shtrikman, J. Mech. Phys. Solids **10** 343 (1962).
[36] J.P. Watt and L. Peselnick, J. Appl. Phys. **51** 1525 (1980).
[37] G. Arlt, J. Mater. Sci. **25** 2655 (1990).
[38] J.F. Nye, *Physical Properties of Crystals* (Oxford University Press, Oxford, 1976).
[39] Y.C. Wang and R.S. Lakes, Q. appl. Math. **63** 34 (2005).
[40] Y.C. Wang and R.S. Lakes, Phil. Mag. **84** 3785 (2004).
[41] M. Brodt and R.S. Lakes, J. Mater. Sci. **31** 6577 (1996).
[42] P.D. Norman, S.W. Wilkins, T.R. Finlayson, *et al*., Scripta Metall. **18** 575 (1984).
[43] N. Toyoshima, K. Harada, H. Abe, *et al*., J. Phys. Soc. Japan **63** 1808 (1994).
[44] R.F. Hehemann and G.D. Sandrock, Scripta Metall. **5** 801 (1971).
[45] S. Kartha, J.A. Krumhansl, J.P. Sethna, *et al*., Phys. Rev. B **52** 803 (1995).
[46] X. Zhou and M. Wuttig, Phys. Rev. B **44** 10367 (1991).